# Creation of Impurity Source inside Plasmas with Various Types of Tracer-Encapsulated Solid Pellet

Naoki TAMURA, Shigeru SUDO, Chihiro SUZUKI and Hisamichi FUNABA

*National Institute for Fusion Science, 322-6 Oroshi-cho, Toki, Gifu 509-5292, Japan*

(Received 29 July 2014 / Accepted 7 April 2015)

A Tracer-Encapsulated Solid Pellet (TESPEL) was developed for promoting an impurity transport study in a magnetically-confined plasma. One of the advantages of the TESPEL is that it can make a three-dimensionally localized impurity source in the plasma. This enables us to inject the tracer impurity inside or in the vicinity of the region of interest. Recently, a new-type TESPEL with a thinner outer shell has been developed in order to achieve a shallower deposition of the tracer impurity. With the TESPEL having the thinner shell, we have achieved about 4 cm shallower deposition of the tracer impurity, compared with the case of the conventional thick-shell type TESPEL with the same outer diameter of about 700 μm. Moreover, for the achievement of the further shallower deposition of the tracer impurity, we also developed the TESPEL with a tracer-impurity-doped thin shell. After the injection of the TESPEL with the tracer-impurity-doped thin shell, the line emissions from the highly-ionized doped impurity are clearly observed with a vacuum ultraviolet spectrometer, which clearly demonstrates its ability to carry the impurity as a new tool.



Keywords: TESPEL, impurity pellet, impurity source, impurity transport

DOI: 10.1585/pfr.10.1402056

## 1. Introduction

In recent studies oriented to a fusion reactor, the importance of knowledge on an impurity behavior in a magnetically-confined plasma is increasingly recognized, since the impurities will play a critical role both in the fuel dilution in a plasma core and the reduction of a heat load on a divertor. Here, it is absolutely essential that the distribution of impurities in both the plasma core and the plasma edge are precisely controlled. Therefore, it is important to gain a full understanding of the impurity transport in the magnetically-confined plasma. However, we still lack understanding regarding the impurity transport in the magnetically-confined plasma. In this situation, a Tracer-Encapsulated Solid Pellet (TESPEL) [1, 2] was developed to promote the impurity transport study in the magnetically-confined plasma. The impurity transport study with the TESPEL technology has been performed mainly in the Large Helical Device (LHD) [3, 4] at the National Institute for Fusion Science (NIFS) in Japan, and is currently planned in the TJ-II stellarator [5] at the National Fusion Laboratory in the Research Center for Energy, Environment and Technology (CIEMAT) in Spain [6]. The TESPEL is a double-layered impurity pellet. In general, the TESPEL consists of a polystyrene $(C_8H_8)_n$ polymer as an outer shell and a tracer impurity as an inner core. This configuration enables us to have the following unique features: a) the TESPEL can produce both a toroidally and a poloidally localized tracer impurity source in the plasma; b) the total amount of the tracer impurity deposited in the plasma can be identified clearly, since the size of the inner core of TESPEL can be measured before the injection; and c) various elements can be selected as the tracer impurity. The first feature makes it possible to inject the tracer impurity inside or in the vicinity of the region of primary interest, such as an internal diffusion barrier (IDB) region, which was discovered in the LHD [7]. In this paper, we present the experimental demonstrations of the creation of the localized impurity source in the plasma with various types of TESPELs, two of which are recently developed.

## 2. Experimental Setup

### 2.1 Experimental apparatus

The LHD with a heliotron type magnetic configuration has superconducting $l/m = 2/10$ helical coils and 3 pairs of superconducting poloidal coils with a magnetic axis $R_{ax} = 3.50$ - $4.05$ m. Here, $l$ and $m$ are a pole number of the helical coil winding and a toroidal field period, respectively. In LHD, the plasma was initiated by an electron cyclotron heating (ECH) [8] and heated additionally by a neutral beam injection (NBI) [9]. Here, hydrogen is used as a working gas. Figure 1 shows a schematic top view of the layout of the main diagnostic apparatus for the TESPEL injection experiment on LHD. The TESPEL injector is installed on the equatorial plane at Port 3-O of LHD and the TESPEL is injected toward the LHD center from the outboard side of the LHD plasma [2]. The pneumatic pipe-gun technique is adopted as a method for in-

*author's e-mail: ntamura@LHD.nifs.ac.jp*

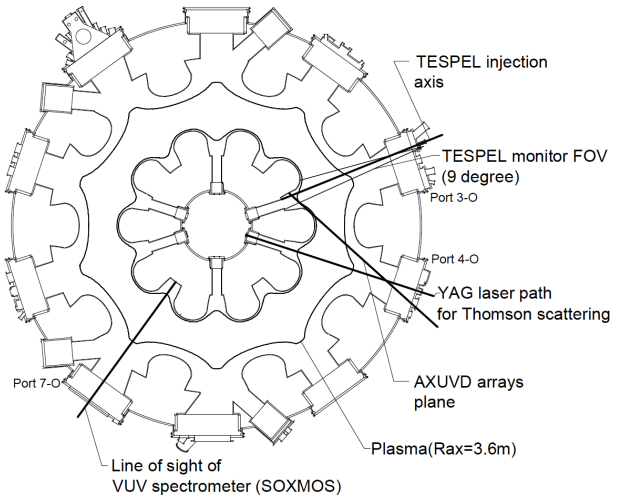


Fig. 1 Schematic top view of the layout of the main diagnostic apparatus for the TESPEL injection experiment on LHD.

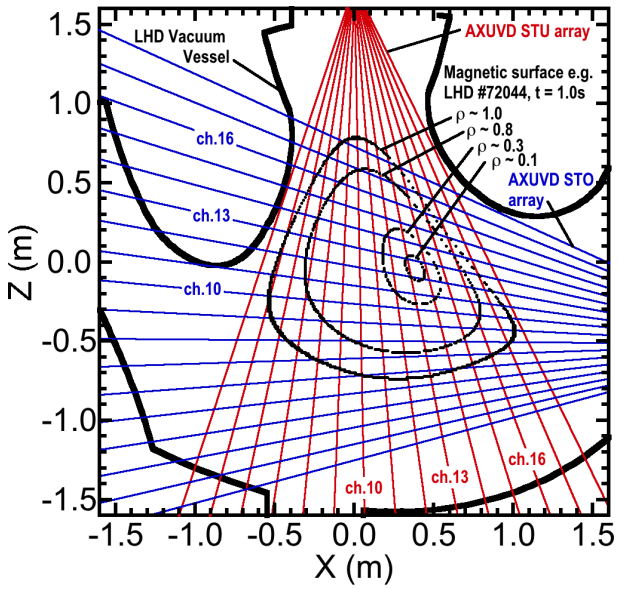


Fig. 2 Layout of the lines of sight of two AXUVD arrays with the LHD vacuum vessel. As a guide, the magnetic surfaces at $\rho \sim 0.1$, 0.3, 0.8 and 1.0 for LHD #72044 at $t = 1.0$ s are also depicted.

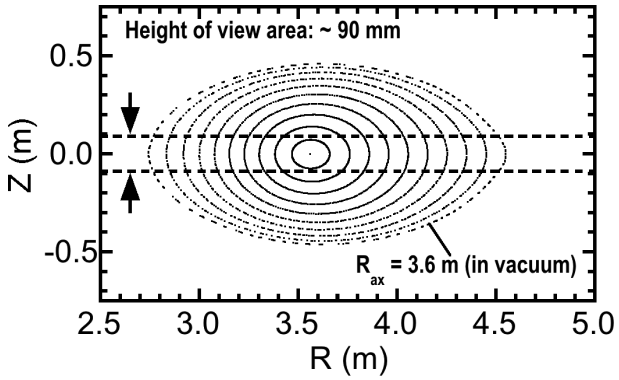


Fig. 3 Field of view of the VUV spectrometer (SOXMOS).

jecting the TESPEL. The TESPEL is accelerated through the gun barrel (an inner diameter of 1 mm and its length of about 410 mm) by helium gas with the typical pressure of 3.5 MPa. In consequence, the TESPEL velocity is typically obtained in the rage of 300 - 400 m/s. This velocity is measured by the time of flight method. In the TESPEL injection system, He-Ne laser sheets are installed at two different locations. When TESPEL interrupts those, the TESPEL velocity can be deduced from the distance between two locations and the difference in the time of interruption. The scattering of the TESPEL trajectory is typically within 1 degree in a full angle. The line emissions from the ablating cloud of the TESPEL injected into the LHD plasma is received with a collector optics (a viewing angle of 9 degree), which is installed at the port adjacent to the TESPEL injection port, through a quartz window, and then is transmitted to a neighboring room by an optical fiber [10]. With the collector optics, the ablation emission from the TESPEL can be measured usually from beginning to end. In the neighboring room, the ablation emission transmitted is measured with photomultiplier tubes (1 MHz sample rate) equipped with appropriate optical filters. Here, the optical filters for Ti I ($\lambda_{\mathrm{center}} = 400.3$ nm, FWHM = 2.0 nm), for H$\alpha$ ($\lambda_{\mathrm{center}} = 657.2$ nm, FWHM = 1.2 nm) and for V I ($\lambda_{\mathrm{center}} = 412.3$ nm, FWHM = 1.1 nm) are used.

A detailed radial profile of electron density $n_{\mathrm{e}}$ and electron temperature $T_{\mathrm{e}}$ along the LHD major radius at a horizontally-elongated cross-section is measured with a YAG Thomson scattering system, which is installed at Port 4-O of LHD [11]. In this system, the number of observation points and typical spatial resolution are 144 and 17 mm, respectively. And the typical temporal resolution is 100 ms, which can be boosted up by changing the combination of the lasers. Total radiated power $P_{\mathrm{rad}}$ is measured by a wide-angle ($2\pi$) metal foil bolometer, which is installed at the same port (Port 3-O) as the TESPEL injector with 5-ms temporal resolution [12]. And plasma radiation is also measured by two 20-channel absolute extreme ultra violet silicon photodiode (AXUVD) arrays, which are installed at Port 3.5-U and Port 4-O on a semi-tangential cross-section in LHD [13]. Figure 2 shows the layout of the lines of sight of the AXUVD arrays with the LHD vacuum vessel. Here, the AXUVD arrays are un-filtered, and thus can observe the plasma radiation, whose energy is ranged from 1.1 eV (visible) to $\sim$ 6000 eV (x-ray) [14]. The temporal resolution of the AXUVD arrays is set at 0.1 ms. The temporal behavior of the emissions in a vacuum ultraviolet (VUV) domain is measured by a 2-m Schwob-Fraenkel soft x-ray multi-channel spectrometer (SOXMOS) [15,16], which is installed at Port 7-O of LHD. Figure 3 shows the field of view of the SOXMOS. The SOXMOS has two micro-channel plates with phosphor screens, which is cou-

pled with a 2048-channel silicon photodiode array through a fiber optic conduit. And then two different spectral domains can be observed simultaneously, but here one of those (from 27.5 nm to 43.5 nm) is analyzed. The temporal resolution (frame rate) of this system is set at 50 ms.

### 2.2 Various types of TESPELs

The firstly-developed TESPEL consists a single and thick shell and a tracer impurity core (hereinafter called a thick-shell type TESPEL). The recipe of the thick-shell type TESPEL is summarized briefly as follows (please see [2] in detail); 1) Drilling a hole on a polystyrene ball; 2) Tracer impurities are loaded into the hole; and 3) the hole is plugged with a tiny polystyrene ball, the outer diameter of which is a slightly smaller than the diameter of the hole as a lid. When the outer diameter of the thick-shell type TESPEL is around 700 μm, the shell thickness of the TESPEL is usually about 250 μm. In this case, the total amount of the electron and ion in the shell are $6.0 \times 10^{19}$ and $1.7 \times 10^{19}$, respectively. Since the typical volume of the LHD plasma is 30 $m^3$, the ratio of the numbers of the electron from this thick-shell type TESPEL to that of the LHD plasma is only 6.7% in the case of the averaged bulk electron density of $3 \times 10^{19}$ $m^{-3}$. Concerning the amount of the tracer impurity in the thick-shell type TESPEL, for example, a titanium Ti of about $3 \times 10^{17}$ particles at a maximum can be loaded into the TESPEL with the size as described above, and thus the electron number, which is introduced by the Ti tracer, is $6.6 \times 10^{18}$ at a maximum (the ratio of that from the Ti tracer to that of the LHD plasma is only 0.7% in the case of the averaged bulk electron density of $3 \times 10^{19}$ $m^{-3}$).

Recently, some of the features of the TESPEL method have been improved. Currently, the region where the tracer was deposited was mainly determined by the outer diameter of the TESPEL. In this case, the smaller TESPEL can contain the lesser amount of the tracer impurity; then we face the problem that the TESPEL for a shallow penetration results in a shortage of the tracer amount for the diagnostics. In order to improve this problem, we developed the TESPEL with the thinner outer shell based on the fabrication technology of a shell type polystyrene $(C_8H_8)_n$ polymer [17]. In the case that the outer diameter of the outer shell is about 700 μm, the thickness of the outer shell is about 70 ~ 80 μm, which is 70% thinner than that with the thick-shell type TESPEL. This configuration is favorable not only for the shallow penetration, but also for the multiplication of the amount of tracer impurity. The recipe of the TESPEL with the thin shell is almost the same as that of the thick-shell type TESPEL as described above. Although the defect in the present process of the TESPEL with the thin shell is that the tiny polystyrene ball as a plug bulged from the surface of the TESPEL, the accelerating performance of such a TESPEL having the bump is comparable to that of the conventional thick-shell type TESPEL.

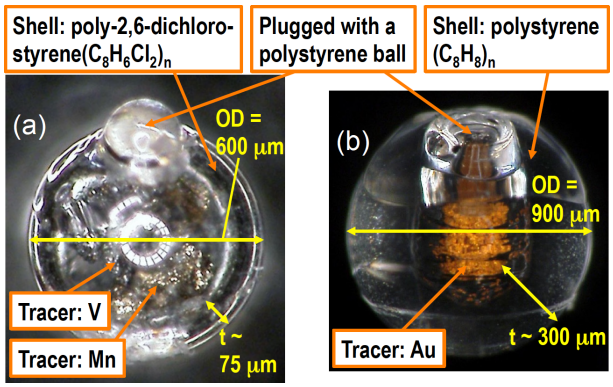


Fig. 4 Photographs of (a) the TESPEL having a tracer-impurity(chlorine Cl)-doped thin shell (OD = 600 μm, shell thickness ~ 75 μm). Here, other tracer-impurities, vanadium V and manganese Mn, are simultaneously loaded into the core region of the TESPEL. For reference, a photo of the conventional (thick-shell type) TESPEL (OD = 900 μm, shell thickness ~ 300 μm) with a gold Au tracer is also shown as (b).

This is because the barrel inner diameter (1.0 mm$\phi$) is much larger than the outer diameter of the TESPEL here (0.6 ~ 0.7 mm$\phi$). For obtaining a further shallower penetration than even with the thin-shell type TESPEL, several TESPEL configurations have been considered. Very recently, one of those, the TESPEL with a tracer-impurity-doped thin shell [18] was realized. In this case, the shell is made of poly-2,6-dichlorostyrene $(C_8H_6Cl_2)_n$, while the previous one is made of polystyrene $(C_8H_8)_n$. Here the chlorine Cl in the shell can also serve as a tracer impurity. Figure 4 (a) shows a photograph of the TESPEL with the thin poly-dichlorostyrene shell. Here, a vanadium V and a manganese Mn clumps are loaded inside the hollow shell for the transport study of multiple impurities. The photograph clearly shows the bulged tiny polystyrene ball from the surface of the TESPEL as described above. For reference, the photograph of the Au-containing conventional (thick-shell type) TESPEL, which is used for the development research of an extreme ultraviolet lithography light source [19], is also shown in Fig. 4 (b).

## 3. Experimental Results

### 3.1 Creation of the localized impurity source with the thick-shell type TESPEL

In order to study precisely the impurity transport in the plasma especially having a characteristic region, the location of the tracer impurity source should be as close to such a region as possible. Because the externally injected impurity from outside the plasma confinement region takes time to reach there, it will be influenced by the transport characteristics in the outer side of the region of interest. Consequently, the effect of the impurity transport characteristic in the region of interest on the exter-

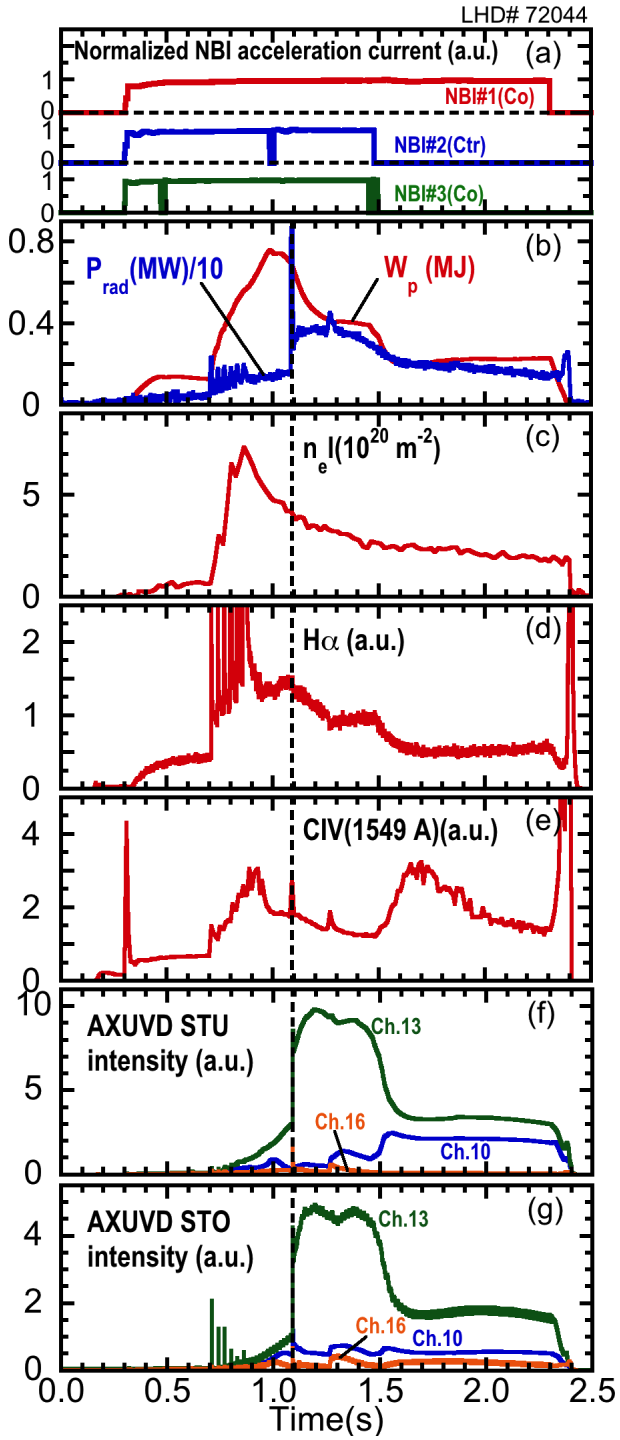


Fig. 5 Typical waveforms of the IDB plasma with the thick-shell type TESPEL injection. A vertical dashed line denotes the TESPEL injection time, $t \sim 1.09$ s.

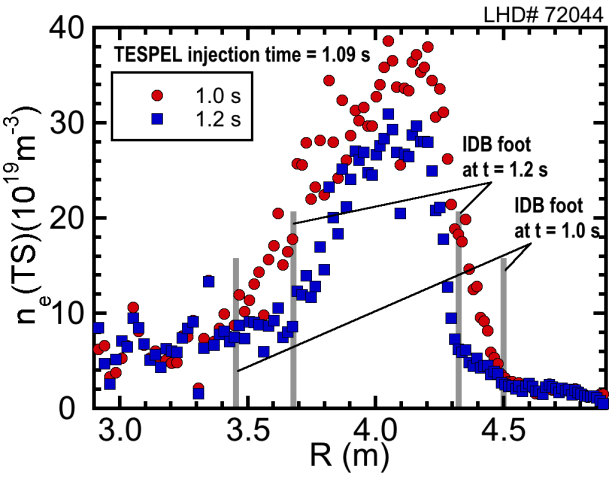


Fig. 6 Radial profiles of electron density measured by the Thomson scattering system before ($t = 1.0$ s) and after ($t = 1.2$ s) the thick-shell type TESPEL injection. Foot points of the IDB are temporarily defined by the location where a sharp bend exists in the electron density profile, which is indicated by gray vertical lines.

nally injected impurity becomes unclear. The ineffectiveness will be more prominent when the characteristic region is located in the deep interior of the plasma, such as the IDB region, which was discovered in the LHD [7]. The TESPEL technology can solve this problem, and is demonstrated here. Figure 5 shows typical waveforms of the IDB plasma with the thick-shell type TESPEL injection. Here, the Ti of about $2 \times 10^{17}$ particles is loaded as the tracer impurity into the TESPEL. In this discharge, a multiple solid hydrogen pellet injection, the time of which is indicated by large spikes in the H$\alpha$ signal shown in Fig. 5 (d), is performed from $t = 0.71$ s to $t = 0.86$ s, and the ultrahigh density region with the IDB is then established. The thick-shell type TESPEL is then injected at $t \sim 1.09$ s as indicated by a vertical dashed line. At this time there is a very sharp peak in the $P_{\rm rad}$ signal. This is because the wide-angle bolometer, which is installed at the same port as the TESPEL injector, can also observe the emissions from the TESPEL ablation cloud. After this sharp peak, the $P_{\rm rad}$ is higher than that during the period from the end of the multiple pellet injection until the time of the thick-shell type TESPEL injection (the period of the IDB plasma without the Ti tracer impurity) and remains at the higher level for about 300 ms. Next, the $P_{\rm rad}$ is then gradually decreased, which is started before NBIs (#2 and #3) are turned off. As can be clearly recognized from Figs. 5 (f, g), the signal intensities of channel (ch.) 13 of the AXUVD array at the upper port (AXUVD STU) and that at the horizontal port (AXUVD STO) after the thick-shell type TESPEL injection are extremely increased, compared to that measured with the wide-angle bolometer, and are sustained until around $t = 1.4$ s. This behavior clearly suggests that the tracer impurity is deposited locally in the core region of the LHD plasma, and is kept in there. In fact, the tracer impurity deposited in the core region of the LHD plasma is immediately affected by the transport characteristics there, which verifies the unique advantage of the TESPEL technology. Figure 6 shows radial profiles of the electron density before (at $t = 1.0$ s) and after (at $t = 1.2$ s) the TESPEL injection. Here, the foot points of the IDB are temporarily

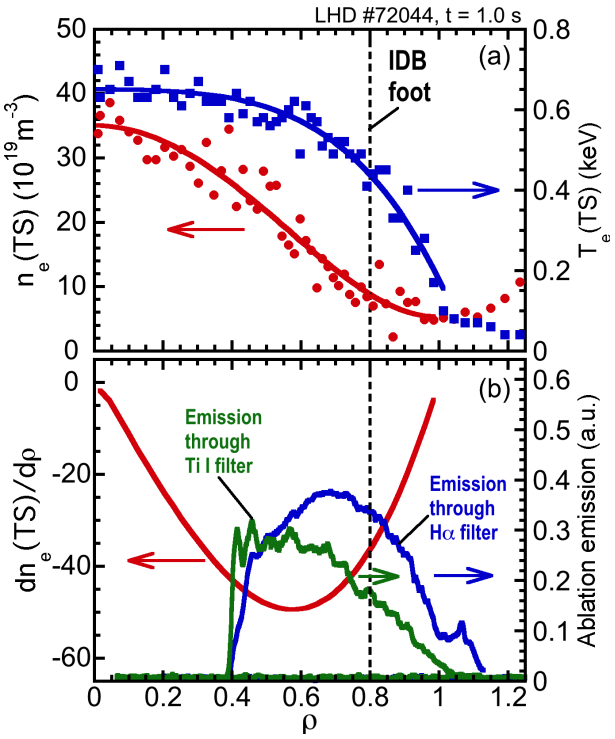


Fig. 7 Normalized radial profiles of (a) electron density and electron temperature measured by the Thomson scattering system at $t = 1.0$ s before the thick-shell type TESPEL injection and (b) electron density gradient and TESPEL ablation emissions. The foot point of the IDB is indicated by a vertical dashed line. Ti tracer impurity is consider to be deposited between $\rho = 0.4$ and $\rho = 0.5$.

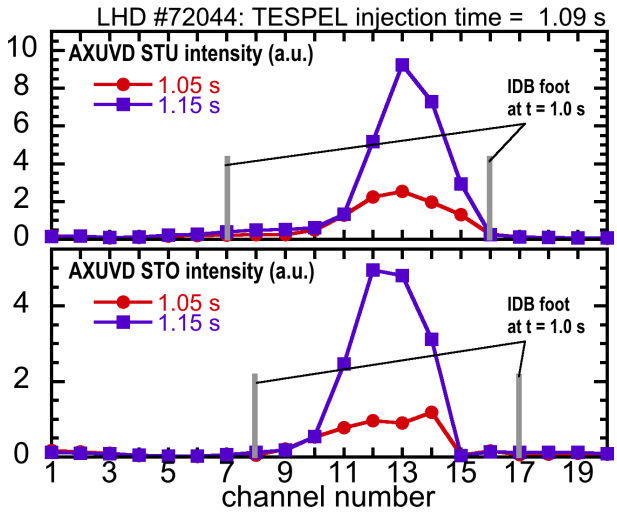


Fig. 8 Channel profiles of the signals from the AXUVD array (a) at the upper port (AXUVD STU array) and (b) at the horizontal port (AXUVD STO array) on the same semi-tangential plane before and after the thick-shell type TESPEL injection. TESPEL injection time is $t \sim 1.09$ s. The foot points of the IDB, which are defined at $t = 1.0$ s, are indicated by gray vertical lines.

defined by the location where a sharp bend exists in the $n_e$ profile [20]. It should be emphasized here that although the higher radiation level is maintained, the injection of the thick-shell type TESPEL containing the tracer impurity does not lead to the dissipation of the IDB and the plasma collapse. Figure 7 (a) shows radial profiles of $n_e$ and $T_e$ at $t = 1.0$ s just before the thick-shell type TESPEL injection. To project the $R$-coordinate on the $\rho$-coordinate (here, $\rho$ is a normalized minor radius), the three-dimensional free boundary MHD equilibrium code VMEC [21] is used. As seen in Fig. 7 (a), the ultrahigh density region can be seen in a wide region of the plasma. (The value of $n_e$ with over $1.0 \times 10^{20}$ m$^{-3}$ is seen inside $\rho \sim 0.75$.) The radial profile of the TESPEL ablation emission can be derived with the TESPEL velocity measured under assumption that the TESPEL moves in a radial direction of the LHD plasma in a state of uniform linear motion. This assumption is generally correct unless the TESPEL trajectory is deflected by an asymmetric ablation process (e.g. due to fast ions). As can be seen in Fig. 7 (b), the thick-shell type TESPEL is found to penetrate deeply inside the IDB plasma. As the TESPEL penetrates deeper into the LHD plasma, the emission through the Ti I filter is gradually increased from the early stage (at this stage, the shell of the TESPEL is still considered to exist, and thus the tracer impurity inside the TESPEL is considered not to expose to the plasma). This is not really the line emission from the Ti tracer impurity, but the continuum emission, which can be also passed through the Ti I filter, from a dense plasma (i.e. ablation cloud) surrounding the TESPEL injected into the LHD plasma. This can be also understood by taking into account very little amount of the tracer impurity, which is three orders of magnitude less than that of the shell material. After the rapid drop of the H$\alpha$ intensity at $\rho = 0.45$, the emission intensity through the Ti I filter is still high. At this stage, the line emission from the Ti tracer impurity is considered to truly appear. Such a change in the dominant emission through the Ti I filter is already confirmed experimentally by a high-time resolved (typical time resolution of 42 μs) spectroscopy with the polychromator equipped with a fast-intensified CCD detector [22] (Here, unfortunately, such data is not acquired). Thus, the Ti tracer impurity is considered to be deposited between $\rho = 0.4$ and $\rho = 0.5$. And consequently, the Ti tracer impurity is set inside the IDB with the TESPEL technology. Figures 8 show channel profiles of the sight-line-integrated signal intensities from the AXUVD STU and the AXUVD STO on the same semi-tangential plane before and after the thick-shell type TESPEL injection. In general, the high-density plasma exhibits the relatively high radiation, i.e., bremsstrahlung radiation. As shown in Fig. 8, in the case of the plasma with the extremely high-density region owing to the IDB, the extremely strong radiation region appears inside the IDB. There is a slight disagreement between the IDB feet and the boundaries of the extremely strong radiation region,

which is more noticeable at the inner channels of the AXUVD STU. This can be attributed to the shrink of the region inside the IDB as already shown in Fig. 6, the effect of the sight-line integration and so on. After the thick-shell type TESPEL injection, the AXUVD signal intensities are dramatically increased only in the region inside the IDB. If the Ti tracer impurity is deposited at the region outside the IDB, the AXUVD signal intensities from such a region should be increased. Therefore the AXUVD array measurements also confirm the successful local deposition of the Ti tracer impurity only inside the IDB region.

### 3.2 Change in the localized impurity source location with the newly-developed TESPEL

Figure 9 shows a comparison result of the deposition location of the tracer impurities between with the thick-shell type TESPEL (LHD #121236) and with the newly-developed thin-shell type TESPEL (LHD #121250). As can be seen from Figs. 9 (a, b), the radial profiles of $n_e$ and $T_e$ of the target plasma for both cases are almost identical. Here, the outer diameter of both TESPELs is the same, ~ 700 μm. As a representative of the loaded multiple impurities, the deposition location of a vanadium V tracer is shown in Fig. 9 (d). Although the acceleration gas pressure is set at the same (2.5 MPa), the resulting velocities of the thick-shell type TESPEL and the thin-shell type TESPEL are 266 m/s and 368 m/s, respectively. From the viewpoint of the TESPEL velocity, the penetration depth of the thin-shell type TESPEL is expected to be deeper than that of the thick-shell type TESPEL. However, as indicated in Fig. 9 (d), with the thin-shell type TESPEL, the location where the V tracer impurity is most deposited is around $r_{\rm eff}/a_{99}(\sim \rho) \sim 0.81$, which is 0.06 in the $r_{\rm eff}/a_{99}$ coordinate shallower than $r_{\rm eff}/a_{99} \sim 0.75$ with the thick-shell type TESPEL (in the real coordinates, ~ 4 cm in $r_{\rm eff}$ shallower deposition of the tracer impurity is achieved.). Here, $r_{\rm eff}$ and $a_{99}$ are the effective plasma minor radius and the effective plasma minor radius, inside which a 99% of the plasma kinetic energy is confined. Typically, the $a_{99}$ can be considered as the position of the Last-Closed-Flux-Surface. (LCFS). As can be confirmed from Fig. 9 (d), the amount of the V tracer inside the thin-shell type TESPEL is surely much increased (here, by a factor of around 2.5), compared with that with thick-shell type TESPEL. Therefore, this result clearly indicates that the flexibility of the TESPEL is successfully expanded with the new thin-shell type TESPEL. Figure 10 shows the experimental results with the TESPEL having the tracer-impurity-doped shell. As can be seen from Fig. 10 (b), the location where the V tracer, one of the centrally-filled tracer impurities, is most deposited can be considered around $r_{\rm eff}/a_{99} \sim 0.82$. Meanwhile, although the ablation emission from the Cl particles in the shell was not measured directly, the Cl tracer impurity in the shell can be expected to be distributed outside

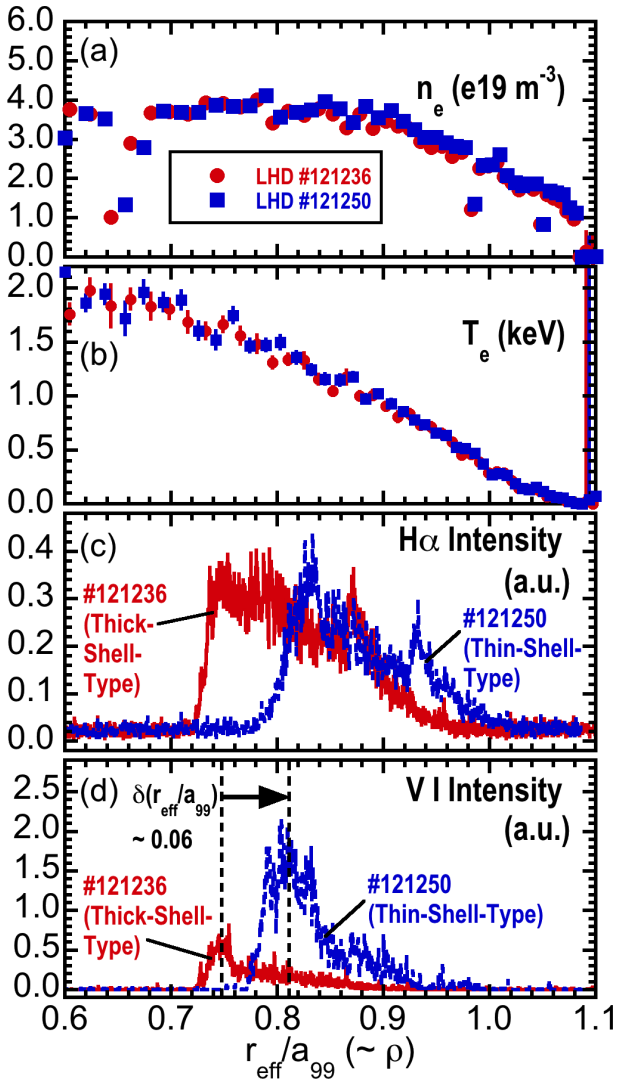


Fig. 9 A comparison result of the deposition location in the normalized minor radius of the tracer impurities between with the conventional (thick-shell type) TESPEL (OD ~ 700 μm, thickness = 200 ~ 250 μm) and with a thin-shell type TESPEL (OD ~ 700 μm, thickness = 70 ~ 80 μm). Here, the characteristic of the vanadium tracer is shown as a representative of the multi-tracer impurities embedded in the core of the TESPEL.

$r_{\rm eff}/a_{99} \sim 0.79$, which is indicated by the radial profile of the emission through the Hα filter shown in Fig. 10 (b) (the shell also contains H). As shown in Fig. 10 (c), the Li-like emission (V XXI, 29.37 nm) from the V tracer impurity ions measured with the VUV spectrometer is drastically increased just after the TESPEL injection and gradually decreased. In the decreasing phase, the decay time is evaluated as $\tau_{\rm decay} = 0.495\,{\rm s} \pm 0.680\,{\rm s}$ with an exponential curve fitting, which is shown as a solid line in the figure. On the other hand, the Li-like emission (Cl XV, 41.56 nm) from the Cl tracer impurity is more quickly increased just after the TESPEL injection. The decay time of the Cl Li-like emission in the decreasing phase, which is also evalu-

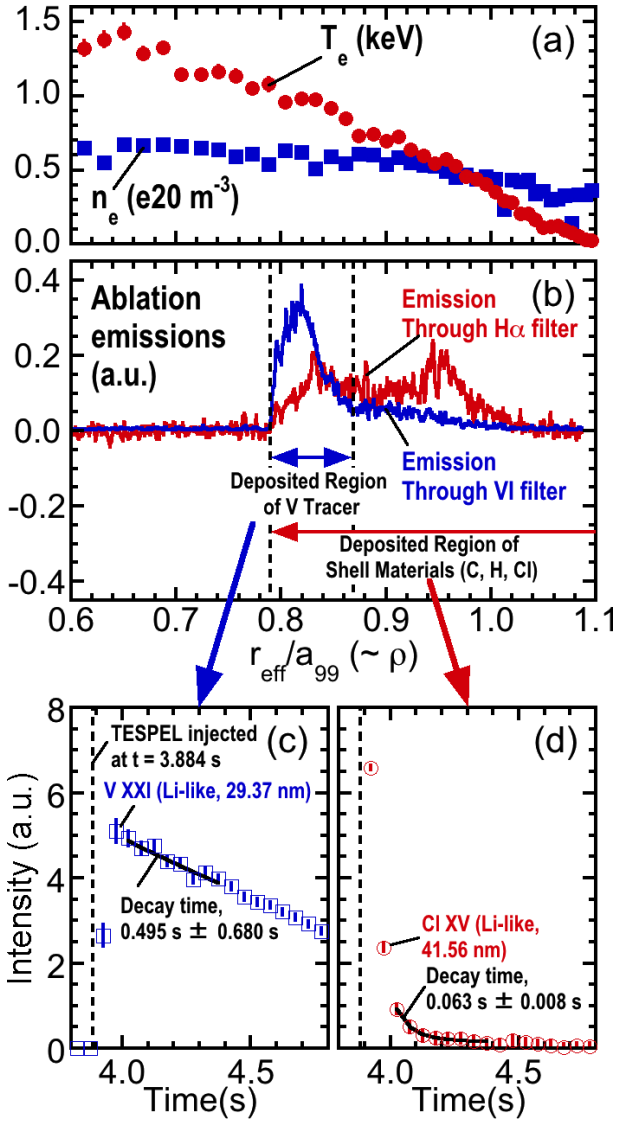


Fig. 10 Experimental result with the TESPEL having a tracer-impurity-doped thin shell (O.D ~ 600 μm, shell thickness = 70 ~ 80 μm). Normalized radial profiles of (a) electron temperature and density of the target plasma, (b) ablation emissions measured through the optical filters for Hα (656.3 nm) and V I (411.2 nm). Temporal evolutions of the VUV emissions (c) V XXI (29.37 nm) and (d) Cl XV (41.56 nm) from the tracer-impurity ions. The exponential fitted solid curves for estimating the decay time are also shown in the figure.

ated from the fitted exponential curve, is 0.063 s ± 0.008 s, which is much shorter than that of the V Li-like emission. Taking the ionization times of the $Cl^{14+}$ and $V^{20+}$ (2.0 ms and 3.7 ms, respectively) into account, the temporal behaviors of the Li-like emissions from both Cl and V ions obtained with the temporal resolution of 50 ms are truly reflected by the transport characteristics. Thus, this experimental result clearly suggests that the impurity transport characteristics inside the layer around $r_{\rm eff}/a_{99} \sim 0.87$ is completely different from that outside the layer, which is recently discovered in the LHD [23,24]. As a consequence, the ability of the TESPEL with the impurity-doped thin shell to carry the impurity as a new tool is clearly demonstrated.

## 4. Discussion

When we intend to inject the tracer impurities into the plasma core even with the TESPEL technology, the $T_e$ of the target plasma has a significant influence on the deposition location of the tracer impurities. The ablation rate of the pellet material can be expressed as $dN/dt = Q(\eta/\varepsilon)$ [25], where $\varepsilon$ is a sublimation energy for a given material, $\eta$ is an attenuation factor of the electron heat flux $Q$, which is indicated by the following formula; $Q \sim 5.01 \times n_e T_e^{3/2} r_p^2 m_e^{-1/2}$. Here, $r_p$ is the ablating pellet radius and $m_e$ is the electron mass. Therefore, the plasma with a lower electron temperature allows the pellet to penetrate deeper. From that point of view, the IDB plasma with the relatively low $T_e$ in the LHD is intrinsically a favorable target for the deposition of the tracer impurities with the pellet technology. Moreover, a large Shafranov shift due to the high pressure at the central region of the IDB plasma makes the magnetic axis of the plasma more outward. This is also favorable point for the deposition of the tracer impurities with the pellet injection that is from the outboard side of the LHD. The outward-shifted configuration of LHD is naturally favorable for the deep penetration depth with the outboard side injection of the pellet. However, the significant point to be emphasized here is that only TESPEL technology can deposit the tracer impurities locally into the region of interest by adjusting the thickness of the shell as demonstrated above.

## 5. Future Works

Concerning the impurity-doped-thin-shell type TESPEL, only the chlorine is tried as the element in the polymer shell at the moment. A fluorocarbon polymer, a compound of fluorine, will be a candidate impurity-doped-shell material. In addition, the polymer doped with nanoparticles of some metal element will be also a possible candidate impurity-doped-shell material. We already made successfully a polystyrene microsphere, the outer diameter of which is around 200 μm, doped with nanoparticles of Mn or Co as the tracer in the TESPEL. There are some technological subjects in forming the shell with the Mn or Co-nanoparticle-doped polystyrene, but it is expected to be available in the near future.

Development of the TESPEL technology is not limited to the TESPEL configuration. The injection technology is also a development object. Currently, the injector, which can make it possible to inject the TESPEL obliquely, is under development. This injector will be able to put the TESPEL injection axis only through the region surrounding the plasma confinement region, namely an ergodic layer. With the utilization of this injector with the

TESPEL having the thin shell or the tracer-impurity-doped thin shell, the tracer impurities can be deposited only inside the ergodic layer. This will be helpful not only for investigating the impurity transport characteristics both in the region just inside the last closed flux surface and in the ergodic layer, but also for controlling precisely the radiation only inside the ergodic layer for the purpose of the reduction of the heat load on the divertor.

# 6. Summary

The creation of the localized impurity source inside or in the vicinity of the region of primary interest in the magnetically-confined plasma has been demonstrated with the various types of TESPELs. The thick-shell type (conventional) TESPEL can deposit the tracer impurity locally inside the internal diffusion barrier observed in the LHD plasma. The thin-shell type TESPEL has been developed in order to achieve the shallower deposition of the tracer impurity. With this type TESPEL, we have achieved about 4 cm shallower deposition of the tracer impurities, compared with the thick-shell type TESPEL having the same outer diameter of about 700 μm. In addition, the tracer-impurity-doped thin shell type TESPEL is also developed for the further shallower deposition of the tracer impurity. The experiment with the tracer-impurity-doped thin shell type TESPEL clearly demonstrates its ability to carry the tracer impurity as a new tool.

# Acknowledgments

The authors acknowledge all of the technical staff of NIFS for their excellent support. This work is partly supported by a Grant-in-Aid for Young Scientists from the Toray Scientific Foundation, a Grant-in-Aid for Scientific Research (B) (Nos. 19340179 and 23360415) from JSPS Japan, and a budgetary Grant-in-Aid of ULHH012 from NIFS.

[1] S. Sudo, J. Plasma Fusion Res. **69**, 1349 (1993).
[2] S. Sudo and N. Tamura, Rev. Sci. Instrum. **83**, 023503 (2012).
[3] O. Motojima *et al*., Phys. Plasmas **6**, 1843 (1999).
[4] O. Kaneko *et al*., Nucl. Fusion **53**, 104015 (2013).
[5] J. Sanchez *et al*., Nucl. Fusion **51**, 094022 (2011).
[6] C. Hidalgo and K. McCarthy, private communication.
[7] N. Ohyabu *et al*., Phys. Rev. Lett. **97**, 055002 (2006).
[8] T. Shimozuma *et al*., Fusion Sci. Technol. **58**, 530 (2010).
[9] Y. Takeiri *et al*., Fusion Sci. Technol. **58**, 482 (2010).
[10] N. Tamura *et al*., Rev. Sci. Instrum. **79**, 10F541 (2008).
[11] I. Yamada *et al*., Fusion Sci. Technol. **58**, 345 (2010).
[12] B.J. Peterson *et al*., Fusion Sci. Technol. **58**, 412 (2010).
[13] B.J. Peterson *et al*., Plasma Phys. Control. Fusion **45**, 1167 (2003).
[14] Datasheet of a 20 ch AXUV photodiode array: http://optodiode.com/pdf/AXUV20ELG.pdf
[15] J.L. Schwob, A.W. Wouters, S. Suckewer and M. Finkenthal, Rev. Sci. Instrum. **58**, 1601 (1987).
[16] C. Suzuki *et al*., J. Phys. B: At. Mol. Opt. Phys. **45**, 135002 (2012).
[17] M. Takagi *et al*., Fusion Sci. Technol. **41**, 278 (2002).
[18] S. Sudo *et al*., Plasma Fusion Res. **9**, 1202082 (2014).
[19] H. Ohashi *et al*., Appl. Phys. Lett. **104**, 234107 (2014).
[20] R. Sakamoto *et al*., Nucl. Fusion **49**, 085002 (2009).
[21] S.P. Hirshman, Phys. Fluids **26**, 3553 (1983).
[22] S. Sudo *et al*., Plasma Phys. Control. Fusion **45**, A425 (2003).
[23] S. Sudo *et al*., Nucl. Fusion **52**, 063012 (2012).
[24] S. Sudo *et al*., Plasma Phys. Control. Fusion **55**, 095014 (2013).
[25] K. Khlopenkov *et al*., Rev. Sci. Instrum. **69**, 3194 (1998).